Article

Doubly Chiral Pseudopeptidic Macrobicyclic Molecular cages: Water-assisted Dynamic Covalent Self-Assembly and Chiral Self-sorting

Ferran Esteve,[1,2] Belén Altava,[1] Eduardo García-Verdugo,[1] Santiago V. Luis,[1,3,*] Jean-Marie Lehn[2,**]

[1]Departamento de Química Inorgánica y Orgánica, Universitat Jaume I, Av. Sos Baynat s/n, Castellón, 12071, Spain

[2]Laboratoire de Chimie Supramoléculaire, Institut de Science et d'Ingénierie Supramoléculaires (ISIS), Université de Strasbourg, 8 allée Gaspard Monge, Strasbourg, 67000, France

[3]Lead contact

*Correspondence: luiss@uji.es

**Correspondence: lehn@unistra.fr

SUMMARY

Taking advantage of the dynamic covalent chemistry approach, four different cages were synthesized by condensation of tripodal pseudopeptides with 4,4'-biphenyldicarboxyaldehyde. Whereas undesired products of polymeric nature were obtained in polar solvents, the [3+2] cryptand-type macrobicyclic architectures were obtained in excellent yields using chloroform as solvent, even at relatively high concentrations. The presence of two encapsulated water molecules may provide a positive template effect in the low polarity medium. The final macrobicycles display a combination of two types of chirality: D,L chirality due to the asymmetric α-C centres and P,M helical chirality. The homochiral helicity found for all the enantiomerically pure molecular cages indicates strong chirality induction by the asymmetric α-C. Besides, the self-sorting properties of the different chiral pseudopeptides have been studied, resulting in high-fidelity homo-self-sorting. DFT calculations point out that the self-sorting outcome may also be a direct result of the encapsulation of two water molecules within the cavity.

Self-sorting, self-assembly, supramolecular, chirality, pseudopeptides, bioinspired, molecular cages, template, macrocyclization, water-assisted

INTRODUCTION

Since the birth of supramolecular chemistry, a wide range of macrocycles and macrobicycles (such as cryptands) have been designed and used for sophisticated applications.[1-4] Nonetheless, the synthesis of preorganized three-dimensional species is generally challenging, as the macrocyclization steps must always overcome the competing oligomerization/polymerization processes.[5-8] Dynamic covalent chemistry (DCC), in particular imine formation, offers a thermodynamically-driven approach that may minimize the generation of such by-products.[9-14] One of the merits of using DCC is that, the reversible nature of dynamic bond allows for the occurrence of component exchange, structural rearrangement and error checking, providing the ideal scenario for self-sorting processes.[15-19]

Several inspiring self-sorting examples have been previously reported based on differences in cation coordination preferences.[20-23] Nevertheless, the assembly of biological supramolecular structures makes mainly use of organic non-covalent interactions such as hydrogen bonding, donor-acceptor interactions and Van der Waals forces.[24] This high-fidelity molecular recognition is responsible for events as crucial as the formation of a DNA double helical structure and the folding of polypeptide chains into proteins with remarkable

The bigger picture

Nature employs elegant pathways to build-up complex architectures, including macrocycles and cages, from simple building blocks. Biological evolution has optimised such processes for affording the desired product with exceptional selectivity, even in highly competing media. Indeed, a well-defined homochirality has been favoured in the construction of macromolecules, with L-amino acids as the main component of proteins and enzymes and D-sugars as the ones for DNA and RNA.

Although there are some significant examples in the literature describing homochiral self-sorting, the bioinspired design herein presented for the synthesis of dynamic pseudopeptidic cryptands may shed light on the complex mechanisms leading to biological homochirality. This work reveals that water encapsulation is essential for the self-sorting outcome, showcasing a non-biological example of the role of water in shaping sophisticated molecules, including their chirality, and therefore mimicking biological behaviours.

selectivity.[25] In conjunction with the forces between components, the medium, in particular water molecules, may serve as supramolecular vectors affecting the stability, structure, dynamics, and functions of biomolecules.[26] Examples of self-sorting experiments between organic components based on such type of supramolecular interactions are rather scarce in the literature.[27-30]

Among the diverse self-sorted examples described to date, chiral self-sorting, i.e., the selection for a supramolecular assembly of an interaction partner with a specific chirality from a complex mixture of possible partners, is of paramount relevance as chirality is an omnipresent property in nature.[31] In fact, in the course of evolution one type of chirality has been favoured in the build-up of the biological molecules making up living organisms, with L-amino acids as the main component of proteins and enzymes and D-sugars as the main components of DNA and RNA.[32] Appropriate design of chiral self-sorting systems may shed light on the formation of complex molecular architectures,[33] allowing for the gradual development of applications involving chiral chemical entities.[34] In this respect, pseudopeptidic compounds could have major advantages, as they present high functional density for potential noncovalent interactions, together with their inherent chirality provided by the amino acid scaffolds.[35] Hence, they could contribute to an understanding of the biomolecular processes.[36]

Herein we report the highly selective formation of cryptand-type macrobicyclic pseudopeptides upon condensation of the tripodal components bearing **L** or **D** valine **V** or phenylalanine **F** amino acid residues (**LTV** / **DTV** / **LTF** / **DTF**) with 4,4'-biphenyldicarboxyaldehyde (**A**) (Scheme 1). These cryptands present enhanced chiroptical properties compared to their corresponding pseudopeptidic precursors because of the higher rigidity prompted by the non-covalent intramolecular interactions. Furthermore, in view of the presence of six imine groups, we have also investigated the DCC behaviour of these novel pseudopeptidic molecular cages in competition experiments with the parent tris(2-aminoethyl)amine (TREN) as well as the related self-sorting properties.

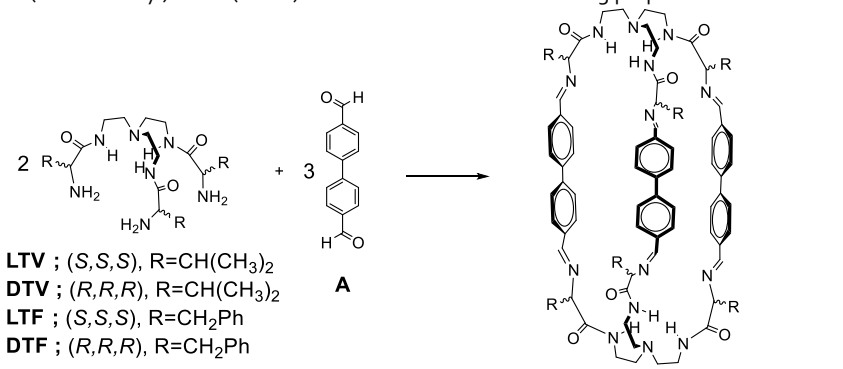

LTV ; (*S,S,S*), R=$CH(CH_3)_2$
DTV ; (*R,R,R*), R=$CH(CH_3)_2$
LTF ; (*S,S,S*), R=CH_2Ph
DTF ; (*R,R,R*), R=CH_2Ph

A

$(LTV)_2A_3$; (*S,S,S,S,S,S*), R=$CH(CH_3)_2$
$(DTV)_2A_3$; (*R,R,R,R,R,R*), R=$CH(CH_3)_2$
$(LTF)_2A_3$; (*S,S,S,S,S,S*), R=CH_2Ph
$(DTF)_2A_3$; (*R,R,R,R,R,R*), R=CH_2Ph

Scheme 1. Molecular structures of the [3 + 2] homoleptic imine-based organic macrobicyclic cryptand cages

Molecular structures of the tripodal pseudopeptides (**LTV, DTV, LTF, DTF**) and the selected dialdehyde (**A**), together with the generated [3 + 2] homoleptic imine-based organic macrobicyclic cryptand cages. **V** (valine) and **F** (phenylalanine) indicate the amino acid used for the preparation of the tripodal pseudopeptidic component. **D** and **L** indicate the amino acid enantiomer used for the preparation of the tripodal pseudopeptidic component.

RESULTS AND DISCUSSION

Synthesis and characterisation of the pseudopeptidic cryptands

The reactions examined involved four pseudopeptidic tripodal compounds derived from natural L-valine and L-phenylalanine, as well as from their corresponding D-enantiomers. The syntheses of the different trisaminoamides followed previously reported procedures.[37]

For the valine derivatives, **DTV** and **LTV**, details of their solid-state structures were established by single crystal X-ray crystallography (Figure S1A and S1B, respectively). Both structures present a highly symmetric fully expanded conformation, with the arms of the pseudopeptide located in the same horizontal plane. The angles between the three different arms are of 112.9(2)º, almost equivalent to the theoretical distribution for a trigonal planar molecular geometry (120.0º). The adoption of such expanded conformation can be explained by the low-energy packing accomplished in solid-state, as the neighbouring molecules of the valine-derived tripodal compounds are interacting by means of parallel intermolecular hydrogen bonding (Figure S1C).[38,39] Indeed, the calculated N···O distance in the solid-state structures for the three symmetric intermolecular hydrogen bonds formed was 2.835(7) Å (HN···O=C bonding, 90% $vdW_{N,O}$).[40,41] Hence, both **LTV** and **DTV** formed β-sheet-like self-assembled crystalline solids.[42,43]

The synthesis of macrobicyclic structures from two tripodal triamine and three dialdehyde components involves the formation of six imine groups by reversible amine-aldehyde condensations in a multiple dynamic covalent process allowing for error correction in the course of the reaction.[13,14,15,17] Despite the unfavourable extended spatial conformation seen in the solid-state for the pseudopeptidic precursors, their capability to form cryptands was evaluated by reacting each of them with 4,4'-biphenyldicarboxyaldehyde (Scheme 1). First, the reaction conditions were optimized using **LTV** as the triamino compound and **A** as the dialdehyde. When the reaction was performed in acetonitrile (3 mM in **LTV** and 4.5 mM in **A**), a substantial polymeric precipitate was formed after 15 h at room temperature. This yellowish material was only soluble in a 50 mol% solution of trifluoroacetic acid in wet $CDCl_3$, allowing for identification of the characteristic ^{1}H NMR signals for **LTV** and **A**. This result agrees with the formation of a highly crosslinked imine-based polymer, undergoing acid-catalysed hydrolysis.[44] Performing the reaction in CD_3CN at 25 ºC allowed real time monitoring the imine formation reactions (Figure S2). After 15 h, some yellowish precipitate was formed, while the solution contained a complex mixture of unreacted reagents (ca. 30%), unidentified intermediates, and 10% of the desired cryptand. After 10 days at room temperature, the reaction led to 14% of unreacted **A** and ca. 30% of $(\mathbf{LTV})_2\mathbf{A}_3$ as the predominant product in solution. The presence of $\mathbf{(LTV)_2A_3}$ was also corroborated by HRMS (Figure S3). Diffusion-ordered spectroscopy (^{1}H DOSY NMR) for the isolated homoleptic L-valine-derived molecular cage provided a diffusion coefficient of $7.08{\cdot}10^{-6}$ cm^2s^{-1} (Figure S4), corresponding to a molecular volume of 3037 Å^3.[45]

When the reaction was performed in $CDCl_3$ at room temperature (3 mM in **LTV**, 4.5 mM in **A**) no precipitation was observed even after 5 days of reaction. ^{1}H NMR revealed the formation of the desired cryptand almost quantitatively (93% NMR yield) after 4 days (Figure 1A). Conversion of **A** was higher than 90% after 8 h, and complete after 20 h. Thus, the consumption of **A** occurred much faster than the appearance of the $\mathbf{(LTV)_2A_3}$ product. This behaviour indicated the occurrence of multiple condensation reactions generating initially different intermediates. This double macrocyclization process was also followed by HRMS analysis. Although HRMS analyses are not fully quantitative, they can be very useful for studying the appearance and disappearance of different components in the course of the reaction.[15] Indeed, Figure 1B shows the relative distribution for the detected intermediates present at different reaction times, together with the formation of the desired [3+2] cage.

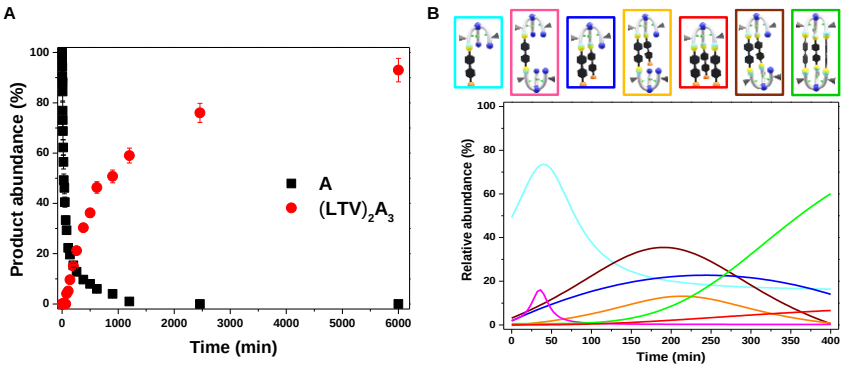

Figure 1. Kinetic profiles for the formation of $(LTV)_2A_3$

(A) Kinetic profile (^{1}H NMR, 400 MHz) for the formation of **(LTV)$_2$A$_3$**. Amount of conversion of **A** and yields for **(LTV)$_2$A$_3$** determined with NMR integration. Reaction conditions: room temperature, 3 mM in **LTV** and 4.5 mM in **A** in $CDCl_3$.
(B) Trends in product distribution calculated for the different reaction times obtained from non-linear fitting of HRMS data.

The evolution with time of the different signals in the ^{1}H NMR spectra afforded valuable information (Figure S5A). After 2 h, once the characteristic signals for the macrobicycle **(LTV)$_2$A$_3$** were well displayed in the spectra, the signal corresponding to water started to shift to higher δ values ($\Delta\delta_{44h}$ = +0.4 ppm, orange discontinuous lines in Figure S5A). This observation suggests the existence of strong interactions between the molecular cage and water molecules, with the hydrophobic medium likely favouring the encapsulation of H_2O molecules tightly hydrogen bonded to the pseudopeptidic moieties of the cage. Therefore, water molecules, as released in the condensation steps, could act as a thermodynamic template,[46,47,6] stabilizing the structure of **(LTV)$_2$A$_3$** and thus favouring its formation, possibly in an autocatalytic fashion.[48,49] No significant shift was observed for water molecules in the experiment in acetonitrile ($\Delta\delta_{10days}$ = +0.02 ppm), suggesting that water templation is much less effective in more polar solvents (Figure S5B).
Due to random twisting motions around the axis of the bridgehead nitrogens, the spectrum of **(LTV)$_2$A$_3$** appears as highly symmetrical, as only a single set of signals is observed, for example, for the imine protons (marked as I in Figure S6) and the proton of the stereogenic carbons (C in Figure S6). The two doublets distinctive of para-substituted aromatic rings (A and B, Figure S6) appearing at 7.42 and 6.48 ppm, respectively, reveal the existence of very different electronic environments for both hydrogen atoms, with one of them substantially shielded. It suggests a significant twisting around the N---N bridgehead axis of the three-dimensional molecular cage with the involvement of π-π intramolecular interactions. It was especially noticeable in the signals of the protons of the methylene group attached to the NH of the amide groups, appearing as diastereotopic protons (E and E′ in Figure S6). The amide protons (D in Figure S6) increase their hydrogen bonding in the cage, as their signal appears at higher δ values than in the open-chain **LTV** (7.98 ppm vs 7.67 ppm, 1.5 mM in $CDCl_3$).
The outcome of the self-sorting in the present system may result from its response to solvent effectors. When the reaction is carried out in a polar solvent such as acetonitrile, products of polymeric nature are generated. Precipitation of such polymers traps the system out-of-equilibrium, and thus without sorted outcome. This shortcoming can be addressed by changing the solvent to chloroform, which keeps the various intermediates in solution and allows for reaching equilibrium, possibly also facilitated by the template effect of encapsulated water molecules, as found in the crystal structures (Figure 2).
Under these optimized conditions, the condensation reactions between **A** and the other pseudopeptidic reagents, **DTV**, **LTF** and **DTF**, were studied separately. All the macrobicyclization reactions afforded the corresponding cryptand with isolated yields higher than 80% for a 3 mM concentration in the triamine (Entries 1-4, Table 1). Interestingly, a 5-fold increase in concentration did not result in any significant decrease in yields (Entries 5-8 in Table 1), emphasizing the robust fidelity of the reagents to self-assemble in such [3+2] architectures. Regarding the effect of changing the amino acid sidechain, slightly better results were observed for phenylalanine derivatives (**(LTF)$_2$A$_3$** and **(DTF)$_2$A$_3$**).

Table 1. Isolated yields obtained in the condensation reactions between A and the four different pseudopeptidic tripodal compounds.

Entry	Macrobicycle	Conc (mM) [a,b]	Isolated yield[c] (%)
1	**(LTV)$_2$A$_3$**	3	85
2	**(LTF)$_2$A$_3$**	3	90
3	**(DTV)$_2$A$_3$**	3	87
4	**(DTF)$_2$A$_3$**	3	92
5	**(LTV)$_2$A$_3$**	15	74
6	**(LTF)$_2$A$_3$**	15	88
7	**(DTV)$_2$A$_3$**	15	81

8	**$(DTF)_2A_3$**	15	90

[a]Solvent: $CHCl_3$, reaction temperature: 25 ºC, reaction time: 5 days.
[b]Concentration of the tripodal open-chain pseudopeptide.
[c] Pure products were isolated after Na_2SO_4 filtration and solvent evaporation, not needing further purification

Crystals suitable for X-ray diffraction were obtained for **$(DTV)_2A_3$**, **$(LTF)_2A_3$** and **$(DTF)_2A_3$**. These solid-state structures provided unambiguous evidence for cage formation (Figure 2). In all cases, the hydrophobic sidechains (isopropyl and benzyl groups for valine and phenylalanine derivatives, respectively) are located in the outer part of the cryptand. In the same way, the three biphenyl fragments are arranged in a helical disposition involving intramolecular π-π interactions. Thus, in the case of **$(LTF)_2A_3$**, the three interacting aromatic bridges adopt two circular edge-tilted-T arrangement with the angles between the centroids of the benzene rings (61.22(2)º, 60.70(2)º, and 58.08(2)º) defining two essentially equilateral triangles (Figure S7A).[50] For each set of three aromatic rings, the smallest intramolecular H_{Ar}-centroid distances were of 2.8321(10), 2.7072(9), and 2.8671(10) Å, corroborating the definition of a slightly distorted equilateral triangle. Overall, the lines connecting the centroids in the two sets of benzene rings identify a Star of David (Figure S7B).[51-53]

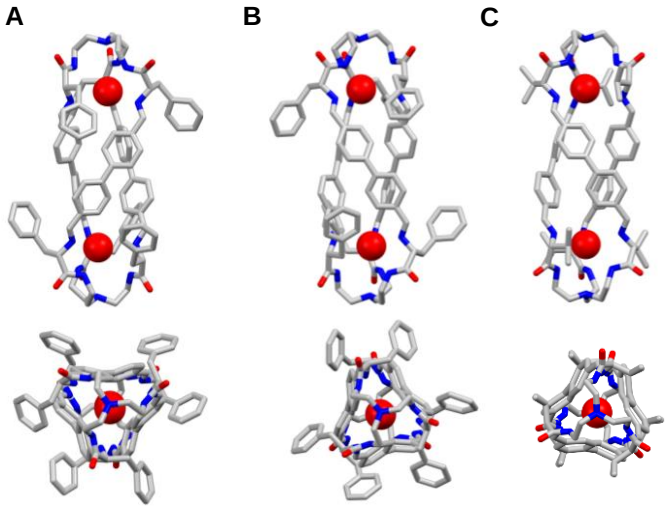

Figure 2. Solid-state X-ray molecular structures of the cryptand-like macrobicyclic pseudopeptides

Solid-state molecular structures of **$(LTF)_2A_3$** and **$(DTF)_2A_3$** and **$(DTV)_2A_3$** (from left to right) showing also the helical chirality enforced by the asymmetric α-C centre as obtained for (A) M-**$(LTF)_2A_3$**, (B) P-**$(DTF)_2A_3$** and (C) P-**$(DTV)_2A_3$**. Side-view (top) and front-view (bottom) have been represented in all cases. Hydrogen atoms, non-essential solvent molecules and disorder have been removed. Oxygen atoms of the encapsulated water molecules have been represented in spacefilling mode for clarity. See supplemental information for crystallographic details.

A similar scenario is found for **$(DTV)_2A_3$**, although in the valine-derived cryptand the shortest H_{Ar}-centroid distances are slightly larger (2.9980(18) Å). These CH···π interactions are in good agreement with the observed ^{1}H NMR shift of the aromatic proton appearing at 6.48 and 6.07 ppm for **$(LTV)_2A_3$**/**$(DTV)_2A_3$** and **$(LTF)_2A_3$**/**$(DTF)_2A_3$**, respectively (Figures S27 and S33). The aromatic sidechains of the phenylalanine derivative also display π-π interactions with the bisphenyl bridging units. The shortest distance between the H_{Ar} of phenylalanine and the closest aromatic carbon of the biphenyl bridge is of 2.731(2) Å. These additional interactions can help to stabilize the three-dimensional structure, explaining the higher yields observed in comparison with the valine derivatives (see Table 1). The polar groups of the pseudopeptidic units are predominantly facing the cavity, creating two hydrophilic pockets in a cage with a strongly hydrophobic surface. Two molecules of water are encapsulated inside the polar terminal pockets (Figures 2 and S8), hydrogen bonded to the

protons of the amide groups (distance $O_{water}\cdots N_{amide}$ = 3.063(6) Å, 97% $vdW_{N,O}$ for **(LTF)$_2$A$_3$**/**(DTF)$_2$A$_3$** and 3.062(5) Å, 97% $vdW_{N,O}$ for **(DTV)$_2$A$_3$**) and with the basic nitrogen atom of the imine groups (distance $O_{water}\cdots N_{imine}$ = 3.050(7) Å, 97% $vdW_{N,O}$ for **(LTF)$_2$A$_3$**/**(DTF)$_2$A$_3$** and 3.037(4) Å for **(DTV)$_2$A$_3$**, 96% $vdW_{N,O}$). This finding is in accordance with water acting as thermodynamic template. Additional intramolecular hydrogen bonds are found between the NH group of the amides and the N atom of the imines, with distances $N_{amide}\cdots N_{imine}$ of 2.732(4) Å (82% $vdW_{N,N}$) for **(LTF)$_2$A$_3$**/**(DTF)$_2$A$_3$** and 2.787(6) Å (84% $vdW_{N,N}$) for **(DTV)$_2$A$_3$** (Figure S8). The intermolecular interactions between water and cage were further corroborated by variable temperature ^{1}H NMR spectroscopy, observing a shift towards lower δ for the water signal and for the NH protons of the amides with increasing temperatures (Figure S9).

Especial attention should be paid to the twisted conformation adopted by the cryptands. Solid-state structures of the pseudopeptidic macrobicycles demonstrate that, in each of the framework of the cages, the three biphenyl units adopt the same rotational conformation, namely either P for clockwise rotation (**(DTF)$_2$A$_3$** and **(DTV)$_2$A$_3$**) or M for anti-clockwise rotation (**(LTF)2A$_3$** and **(LTV)$_2$A$_3$**). Each homoleptic cage thus has helical homochirality, namely P3 or M3,[54-55] which is driven by the orientation adopted by the three aromatic units because of the aforementioned intramolecular CH···π interactions. This propeller-shaped central aromatic moiety can find similarities with secondary structures found in nature,[17,56] as for example the DNA triple helix or the collagen triple helix.[57-59]

We envisaged at this point that such chiral environment should result in strong CD differences for the cryptands. The two enantiomers for each pseudopeptidic cage presented mirror-like CD spectra (Figure 3), expressed through a cotton effect centred at 309 nm, corresponding to the UV absorption for the conjugated central aromatic units.[60-62] The Cotton effect was positive in the case of the homoleptic L-cryptands (**(LTF)2A$_3$** and **(LTV)$_2$A$_3$**) and negative for their enantiomeric molecular cages (**(DTF)$_2$A$_3$** and **(DTV)$_2$A$_3$**). Hence, the helical arrangement was endowed by the intramolecular and intermolecular (with water) supramolecular interactions and the rotational homochirality, was governed by the chirality of the initial pseudopeptide. It agrees with the solid-state structure for the pseudopeptidic based cryptands compared to that reported for the cage prepared from TREN and **A**, in which the bridging units were barely twisted.[17]

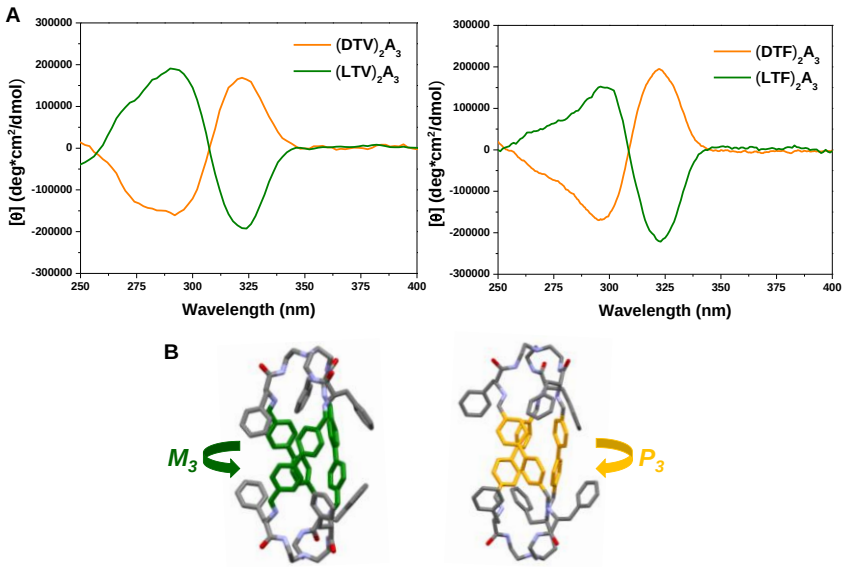

Figure 3. Experimental evidences for the strong helical homochirality induction governed by the α-C chirality

(A) CD spectra comparison ($CHCl_3$, 0.015 mM, 25 °C) for **(LTV)$_2$A$_3$** / **(DTV)$_2$A$_3$** (left) and **(LTF)$_2$A$_3$** / **(DTF)$_2$A$_3$** (right). The superposition of the spectra for each separated enantiomer reflects mirror-like CD.

(B) Representation of solid-state structures found for **(XTF)2A3** (**X**= **D** or **L**) showing the helical chirality enforced by the asymmetric α-C chirality: M-**(LTF)$_2$A$_3$** (left) and P-**(DTF)$_2$A$_3$**

(right). Solvent molecules and hydrogen atoms have been removed for clarity. The aromatic biphenyl bridges have been coloured depending on the rotational chirality

Competition studies with the parent achiral component TREN (T)

After the successful synthesis, isolation, and characterisation of the four homoleptic cages $\mathbf{X_2A_3}$ (**X** = **LTV**, **DTV**, **LTF**, **DTF**), we carried out competition experiments for two different tripodal amines: **LTV** and tris(2-aminoethyl)amine (TREN, **T**). One may consider **T** to be more reactive than **LTV**, as the steric hindrance resulting from the α-substitution in the pseudopeptide might decrease its reactivity. Besides, the nitrogen atoms of the terminal amino groups in **LTV** could be acting as hydrogen bond acceptor in intramolecular interactions, decreasing their nucleophilicity. The initial experiment involved a 3 : 2 : 2 mixture of **A** (4.5 mM), **T** (3 mM) and **LTV** (3 mM) using $CDCl_3$ as solvent (Figure 4).

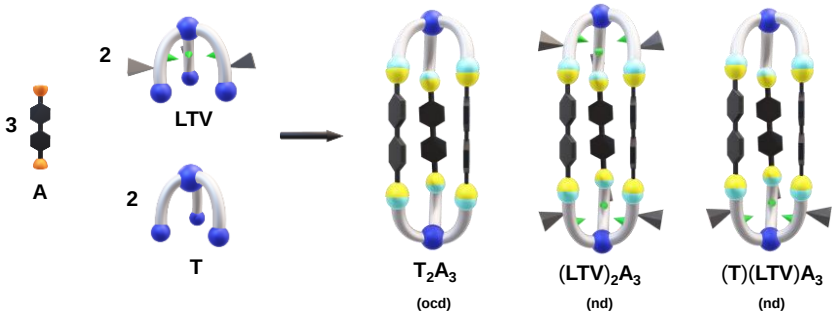

Figure 4. Competition experiment between T and LTV using A as the dialdehyde

Competition experiment between **T** and **LTV** using **A** as the dialdehyde. Reaction conditions: $CDCl_3$, 25 °C, 3 mM for **LTV**, 3 mM for **T**, 4.5 mM for **A**. The abundance of each species was determined by NMR integration. Note: (ocd), only compound detected; (nd), not detected.

In line with the expected tendency, the only cryptand appreciably present in solution after 41 h of reaction was $\mathbf{T_2A_3}$, with all the initial **T** reagent being consumed (Figure S10). In good agreement with this result, the homoleptic cage $\mathbf{(LTV)_2A_3}$ and the mixed heteroleptic cage $\mathbf{(T)(LTV)A_3}$ were not detectable in the ^{1}H NMR spectrum, whereas 95% of the initial **LTV** was still present unreacted. Comparing the kinetic profiles for each separated macrocyclization, noteworthy differences were observed. For instance, the consumption of the aldehyde was slightly faster in the presence of **T** than for its competitor **LTV**, confirming the higher nucleophilicity of **T** over the open-chain tripodal pseudopeptide (Figure S11A). In terms of the yield for the respective cages, the formation of $\mathbf{T_2A_3}$ was also kinetically favoured, as yields higher than 50% were achieved after only 50 min, while it took 600 min for reaching such yields for $\mathbf{(LTV)_2A_3}$ (Figure S11B). The product distribution was stable for more than 10 days, without any exchange between components occurring. This observation suggested that the homoleptic cage $\mathbf{T_2A_3}$ was also the thermodynamically favoured product.

Effect of the sidechain in the self-sorting between components

The effect of the amino acid sidechain in the reactivity and self-sorting properties of the cryptands was also studied. This experiment seemed more challenging, as the reactivity of the tripodal pseudopeptides **LTV** and **LTF** was expected to be similar. The self-sorting experiment was performed using a 2 : 2 : 6 mixture (**LTV** : **LTF** : **A**) in $CDCl_3$ at room temperature (Figure 5A). Monitoring the product distribution by ^{1}H NMR spectroscopy showed that the homoleptic cage $\mathbf{(LTV)_2A_3}$ was formed prior to the homoleptic $\mathbf{(LTF)_2A_3}$ one (Figure 5B), the NMR yields being respectively 11% and 5% after 4 h. In addition to the characteristic peaks of the homoleptic cages, a new signal at 6.20 ppm was assigned to the heteroleptic $\mathbf{(LTV)(LTF)A_3}$ species. The final ^{1}H NMR spectrum indicated that these three products embraced a statistical distribution, namely 1:2:1, as confirmed by NMR integration. The same statistical distribution was also observed in the HRMS analysis of the crude after 10 days of reaction (Figure S12). This result highlights that the sidechain did not trigger significant changes in the energy distribution between homoleptic and heteroleptic compounds.

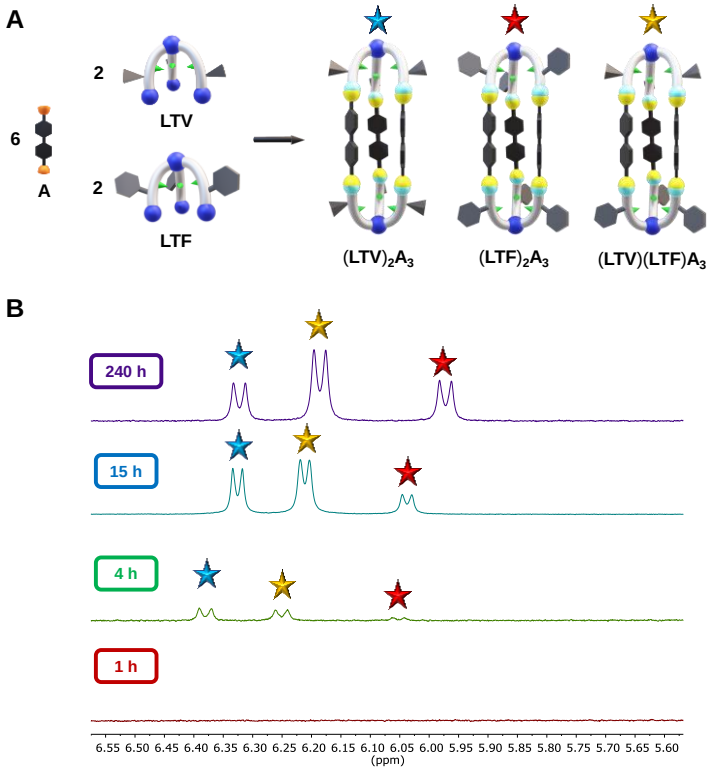

Figure 5. Self-sorting experiment between LTV and LTF using A as the dialdehyde

(A) Representation of the self-sorting experiment between **LTV** and **LTF** using **A** as the dialdehyde. Reaction conditions: $CDCl_3$, 25 °C, 3 mM for **LTV**, 3 mM for **LTF**, 9 mM for **A**. (B) Partial ^{1}H NMR (400 MHz, $CDCl_3$, 25 °C) spectra for the self-sorting experiment at 1 h (red spectrum), 4 h (green spectrum), 15 h (light blue spectrum) and 240 h (purple spectrum).

To probe whether the distribution observed for the self-sorting experiment corresponded to the thermodynamically favoured distribution, we envisaged that mixing two equimolar solutions of pure **(LTF)$_2$A$_3$** and **(LTV)$_2$A$_3$** should result in the formation of the heteroleptic cage over time. This process would be possible through component exchange in presence of a nucleophile or hydrolysis and further rearrangement of the components, permitted by the dynamic nature of the imine bonds. Similar exchange processes have been already established for dynamic macrocycles and cryptands.[15,17] Thus, pseudopeptides **LTV** and **LTF** were first reacted separately with **A** (3 mM for the pseudopeptide and 4.5 mM for the dialdehyde, $CDCl_3$, 25 °C) for 72 h prior to combining the two reaction samples. The resulting mixture was left to equilibrate, monitoring the change in the product distribution over 12 days (Figure S13). The increase in concentration of **A** over time suggested that the error-checking was occurring through hydrolysis and further rearrangement of the components. Although the self-sorting experiment was not completed in the time-range monitored, a final distribution of 30 : 33 : 37 was observed for **(LTV)$_2$A$_3$** : **(LTV)(LTF)A$_3$** : **(LTF)$_2$A$_3$**, suggesting that the three cryptands presented similar energies. HRMS analysis of the final reaction mixture (12 days of reaction) corroborated the formation of the heteroleptic cryptand (Figure S14).

Performing the competition experiment in the presence of a defect of dialdehyde (3 mM for **LTV**, 3 mM for **LTF** and 4.5 mM for **A**), the kinetic preferences of the macrocyclization were also determined (Figure S15A). The signals characteristic of **(LTV)$_2$A$_3$** were the first to be detectable in the ^{1}H NMR spectra (Figure S15B). The heteroleptic cage was the second macrobicycle to be formed, whereas the homoleptic **(LTF)$_2$A$_3$** cage was only detected after 8 h. The corresponding kinetic profiles suggest that the pseudopeptide **LTV** must be somewhat more nucleophilic and/or less sterically hindered than **LTF** (Figure S15C). The kinetic profiles for the separated synthesis of **(LTF)$_2$A$_3$** and **(LTV)$_2$A$_3$** confirmed the higher

reactivity of **LTV** as indicated at short times by the faster consumption of **A** (Figure S16). Inspired by previous studies where the introduction of external chemical species resulted in interesting changes in selectivity,[63-65] the effect of anionic species as chemical effectors in the competition experiment was assayed, but only minor changes were observed in the final distributions after 8 days of reaction (Table S1).

Effect of component chirality in the self-sorting processes

The macrobicyclic compounds **(LTX)$_2$A$_3$** and **(DTX)$_2$A$_3$** (**X**=**V** or **F**) combine remarkable chirality features of two types: asymmetric α-C D,L chirality and helical P,M chirality due to twisting around the N---N bridgehead axis enforced by the asymmetric α-C centre in opposite directions for D and L. Figures 2 and 3 show the corresponding molecular structures in the solid-state for M-**(LTF)$_2$A$_3$**, P-**(DTF)$_2$A$_3$** and P-**(DTV)$_2$A$_3$**. These observations, together with the spectroscopic data found, suggest a strong helical chirality induction.[66,67] A related homochiral induction by asymmetric α-C centers is found in trinuclear double stranded helicates,[68] and in the formation of chiral tetrahedral cages.[69]

The information gathered from ^{1}H NMR, CD and solid-state analyses, indicated that the helical macrobicycles here described could promote chiral self-sorting. Several examples can be found in the literature describing homochiral rearrangements in the syntheses of highly twisted molecules or pinwheel-shaped structures.[70-72] The formation of helical architectures generally results in homo-self-sorting, as the arrangement in the heteroleptic species would always lead to a helical conflict, coming at high energy costs.[32]

The self-sorting between **LTV** and **DTV** was first considered. Reacting a mixture of the enantiomeric tripodal pseudopeptides with **A** could produce either homochiral (homo-self-sorting) or heterochiral (hetero-self-sorting) macrobicycles (Figure 6).[73,74] The heterochiral **(LTV)(DTV)A$_3$** assembly represents the unusual case of a triple stranded meso structure, diastereomeric with respect to the homochiral assemblies.

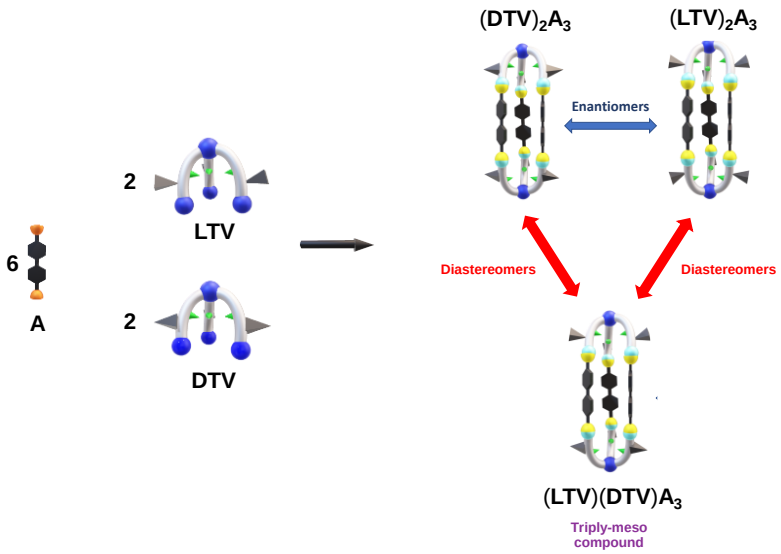

Figure 6. Self-sorting experiment between LTV and DTV using A as the dialdehyde

Self-sorting experiment between **LTV** and **DTV** using **A** as the dialdehyde, leading to two homochiral enantiomers **(DTV)$_2$A$_3$**, **(LTV)$_2$A$_3$** and a heterochiral triply-meso diastereomer **(LTV)(DTV)A$_3$**. Reaction conditions: $CDCl_3$, 25 °C, 3 mM **LTV**, 3 mM **DTV**, 9 mM **A**.

It must be noted that ^{1}H NMR spectroscopy can only quantify the homochiral/heterochiral ratio, namely (**(LTV)$_2$A$_3$** + **(DTV)$_2$A$_3$**) / **(LTV)(DTV)A$_3$**. ^{1}H NMR spectra for the reaction mixture at different times (Figure S17) allowed identifying new signals assignable to the heterochiral cage. After 19 h of reaction, a product distribution of 59 : 41 (homochiral : heterochiral) was determined, the homochiral being favoured. Thereafter, a progressive decrease in the concentration of the heterochiral species was observed over time (Figure S18). After 13 days at room temperature, the heterochiral cage was still present in the reaction mixture, with a

90 : 10 homo- to heterochiral ratio. HRMS analyses corroborated that the major compounds during the rearrangement were the homochiral/heterochiral cages of same mass, being the three components characterised by m/z peaks at 1410.9 and 705.4 m/z, for $[M+H]^{+}$ and $[M+2H]^{2+}$ respectively (Figure S19). Carrying out the experiment in the presence of 10 mol% of TFA resulted in a ca. 2.6 times faster homochiral self-sorting, as the redistribution was catalysed by the acid (Figure S20).

Interestingly, one of the signals assigned to the aromatic protons of the biphenyl groups of the heterochiral cages did not show the characteristic δ shift observed in homochiral cryptands (compare B and B′ signals in Figure S21). This suggests that the heterochiral species does not induce a helical twisting with π-π stacking as a result of the opposite twisting preference of the heterochiral (**LTV**) and (**DTV**) lids. The self-sorting process should be even more efficient between **LTF** and **DTF**, as these phenylalanine-derived macrobicycles presented a more pronounced helical conformation due to the additional π-interactions with the aromatic sidechains. In agreement with this hypothesis, when reacting a **LTF** : **DTF** : **A** mixture (2 : 2 : 6 equivalents respectively) the evolution of the peaks for the different species showed a significantly faster rearrangement, shifting from an initial 60 : 40 homochiral : heterochiral distribution to the final 96 : 4 distribution in less than 3 days (Figure S22).

DFT calculations for the homochiral and heterochiral macrobicylic cages were carried out to estimate energy differences for valine and phenylalanine derivatives. All conformation optimizations were calculated for the isolated molecules, providing endergonic formation energies for the cryptands (Figure 7A). Energy diagrams for the isolated compounds do not agree with experimental results, as, for instance, the heterochiral cage was calculated to be almost 10 kcal/mol more stable for the valine cryptand. However, taking into account the observed binding of water molecules inside the cavity of the ditopic cryptand cage, the energies for the most stable conformation of the macrobicycles were calculated with two molecules of water encapsulated within the hydrophilic pockets (Figure 7B). The trapped water molecules were clearly stabilizing the homochiral cages, decreasing their energy by 15.2 and 10.6 kcal/mol for $\mathbf{(LTV)_2A_3}$ and $\mathbf{(LTF)_2A_3}$, respectively. This stabilization was much lower for the heterochiral cage, in which the weaker host-guest noncovalent interactions barely modified the initial energy (< 2 kcal/mol). This role of the water molecules was confirmed by ^{1}H NMR experiments, revealing a significant shift towards higher δ values of the water signal as the system underwent the heterochiral to homochiral change (Figure S23). It must be noted that the encapsulation of water seemed more efficient for the valine cryptand, $\Delta\delta_{H2O}$ = +1.1 ppm for $\mathbf{(LTV)_2A_3}$ and +0.35 ppm for $\mathbf{(LTF)_2A_3}$, which correlates well with the energy reduction estimated upon water binding.

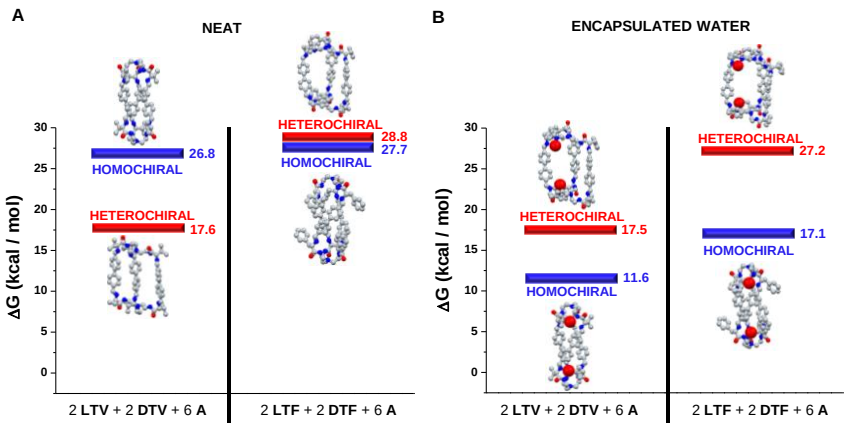

Figure 7. DFT calculated conformations and energies for the cryptands

Most stable conformation (DFT, B3LYP, LANL2DZ, Gaussian09) for the homochiral and heterochiral cryptands (A) in the absence and (B) in the presence of two water molecules. Free energies (kcal/mol) have been calculated from the formation energies of the reaction components. See computational section in supplemental information for more details

The energy differences between the homochiral and heterochiral cages in the presence of water were of 5.9 and 10.1 kcal/mol for the valine and phenylalanine macrobicycles

respectively. These values are in agreement with the self-sorting experiments for the systems, revealing a higher predominance of the homochiral cage -under the same conditions- for the phenylalanine derivative (Figures S18 and S22). These results indicate that the encapsulation of water played a crucial role in the self-sorting outcome, showcasing a non-biological example of the role of water in shaping sophisticated tertiary and quaternary structures found in proteins.[75]

The former results highlight the key role of the side chain of the constituent amino acid in these processes. The efficient encapsulation of H_2O can be associated to the hydrophobicity of the sidechains in Val and Phe derivatives. The higher efficiency observed for Val can reflect the higher hydropathy of its sidechain.[76] It must be noted, besides, that the folding of the benzyl group to maximize the aromatic-aromatic interactions leads to a less efficient hydrophobic shielding of the pseudopeptidic fragment interacting with the water molecule in $\mathbf{XTF_2A_3}$ and can also disturb the hydrogen bond interactions associated to this encapsulation. Hence, the strong hydrophobic surface of $\mathbf{XTV_2A_3}$ can enhance water encapsulation and, thus, homo-chiral self-sorting. It must be noted that experiments carried out with the tripodal triamine derived from glycine (less hydrophobic[76] but also lacking chirality) did not produce in an efficient way the desired molecular cages (only complex mixtures of products were obtained). Similar results were obtained with the triamino compound derived from tryptophane (significantly more hydrophilic according to the same scale)[76], but it is worth mentioning that results from Trp derived triamine must be handled carefully as much as the large aromatic unit in the sidechain can also participate in aromatic interactions and contains a H-bond donor fragment.

Considering this effective chiral self-sorting, one may surmise that the same pronounced helical twisting induced by the chiral centers could also affect the self-sorting of two tripodal pseudopeptides with different sidechains and opposite chirality. When components **LTV**, **DTF** and **A** were mixed in a 2 : 2 : 6 ratio in $CDCl_3$, the self-sorting of the system was clearly apparent in the ^{1}H NMR spectra. Figure 8 shows the evolution of the spectra over time, with the formation of both $\mathbf{(LTV)_2A_3}$ and $\mathbf{(DTF)_2A_3}$. In excellent accordance with the kinetic preferences of **LTV** over **DTF**, the $\mathbf{(LTV)_2A_3}$ macrobicycle was formed earlier than its phenylalanine analogue. The spectrum of the reaction outcome after 3 days was a superimposition of the spectra from the individual reactions for the preparation of the homoleptic/homochiral cryptands under similar experimental conditions, revealing the absence of heteroleptic cage $\mathbf{(LTV)(DTF)A_3}$. This efficient self-recognition process was confirmed by HRMS analysis, observing that after 78 h the two major products were the homoleptic cages, with only traces of the heteroleptic species detected (Figure S24).

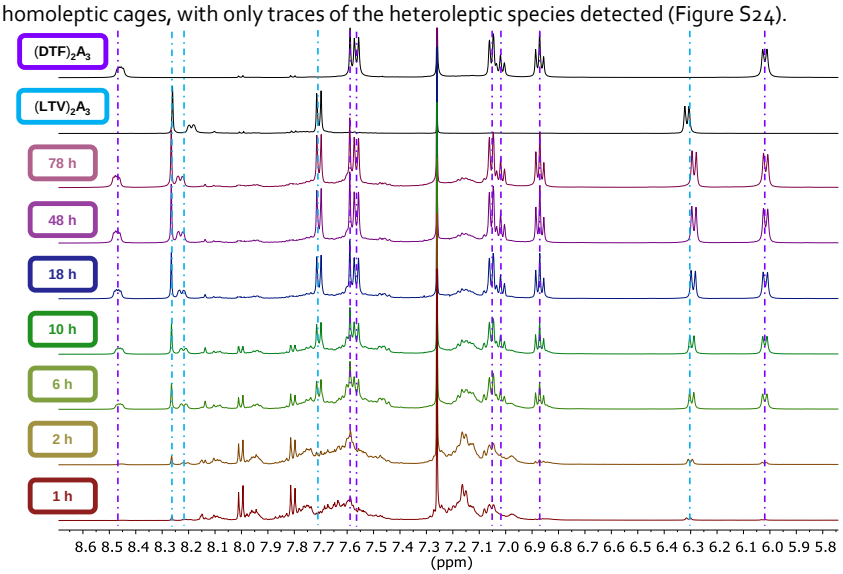

Figure 8. Self-sorting experiment between LTV and DTF using A as the dialdehyde

Partial ^{1}H NMR (500 MHz, $CDCl_3$, 25 °C) spectra for the self-sorting experiment at different times. Reagents: **LTV**, **DTF** and **A** (3 mM, 3 mM and 9 mM, respectively). The two black

spectra on top correspond to the pure macrobicycles (1.5 mM each), highlighting the signals for **(LTV)$_2$A$_3$** (blue lines) and **(DTF)$_2$A$_3$** (purple lines).

The intramolecular noncovalent forces, and thus the helical chirality of the architecture, appear to be responsible for reaching such high-fidelity self-sorting. Performing the process with the alternative mixture of compounds, namely **DTV** : **LTF** : **A** reacting in a 2 : 2 : 6 ratio, resulted as expected in the same homo-self-sorting, with the spectrum of the final reaction mixture being a superimposition of **(DTV)$_2$A$_3$** and **(LTF)$_2$A$_3$**. Therefore, the intrinsic chirality of the secondary structure was able to promote excellent selectivities in the self-sorting between components. As evidence of chirality driven self-recognition, when all four tripodal reagents were mixed in the presence of **A** in a 2 : 2 : 2 : 2 : 12 ratio (**LTV** : **DTV** : **LTF** : **DTF** : **A**), the statistical distribution previously observed for the sidechain self-sorting experiment (see for instance Figure 5) was obtained (Figure S25). Hence, the system was able to perform chirality self-sorting towards homochiral compounds but did not distinguish between the sidechains of the valine or phenylalanine derived species.

Conclusions

In conclusion, the work presented herein describes the efficient synthesis of novel chiral pseudopeptidic macrobicycles. Whereas products of polymeric nature are favoured in polar solvents, the cage structure is obtained in almost quantitative yields in homogeneous solution where equilibrium can be achieved. This high efficiency is due to a large extent to the positive template effect of water molecules bound in the three-dimensional cavities formed by the tripodal capsules at each end of the macrobicyclic structure, as revealed in the solid-state by radiocrystallography and ^{1}H NMR spectroscopy. The present pseudopeptidic cages display helical chirality and a preorganized cavity for molecular recognition of polar substrates in hydrophobic media, adding value to their straightforward synthesis via imine condensation.

The pseudopeptidic dynamic library responded primarily to chirality features, as high-fidelity chiral homo-self-sorting was achieved for the mixtures. Such fidelity is remarkable for such complex multicomponent systems made up from purely organic building blocks that differ in chirality, with structures presenting similar binding sites. The encapsulation of discrete water molecules appears to be the main driving force for this error-checking process, thus stressing the role of the aqueous medium in the formation efficiency and selectivity as well as in the determination of structural features of complex three-dimensional architectures in biomolecules.

EXPERIMENTAL PROCEDURES

Resource availability

Lead contact

Further information and requests for resources and reagents should be directed to and will be fulfilled by the lead contact, prof. Santiago V. Luis (luiss@uji.es).

Materials availability

All materials generated in this study are available from the lead contact upon request.

Data and code availability

Data and code generated during this study are available from the lead contact upon request.

Instrumentation and Measuremets

NMR spectra were recorded on Bruker Avance 400 (400 MHz for ^{1}H and 100 MHz for $^{13}C\{^1H\}$), Bruker Avance III plus 400 (400 MHz for ^{1}H and 100 MHz for $^{13}C\{^1H\}$), and Bruker Ascend Spectroscope Avance Neo-500 MHz (500 MHz for ^{1}H and 125 MHz for $^{13}C\{^1H\}$) instruments. MestReNova 10 software was used for the treatment of the NMR spectra. Chemical shifts are given in ppm. Residual solvent peaks were taken as reference ($CDCl_3$:7.26 ppm). NMR tubes were sealed with Teflon caps to avoid evaporation of solvent and changes in concentration. Quantitative ^{1}H NMR were measured using the integration of the residual solvent peaks as

internal standard. The error in ^{1}H NMR integration amounts to ± 5% (the error bars in the quantitative NMR graphs account for 5% of each data point). The coupling constants (J) are listed in Hz. Peaks are described as singlet (s), doublet (d), triplet (t), doublet of doublets (dd) and multiplet (m). Unless otherwise noted, spectra were recorded at 25 °C.

HRMS-ESI (High-Resolution Mass Spectrometry-Electro-Spray Ionisation) mass spectra were recorded by direct injection into a ThermoFisher Exactive Plus EMR Orbitrap mass spectrometer. The CD spectra were recorded on CD-ORD J-1500 (Jasco).

Commercially available chemicals were purchased from Sigma-Aldrich, Alfa Aesar, Fluorochem, TCI and were used without further purification. Solvents and reagents of pharmaceutical grade quality were purchased from Carlo Erba, and solvents of spectroscopic grade were purchased from Sigma-Aldrich and Fisher Chemical. $CDCl_3$ was purchased from Euriso-TOP and filtered through basic alumina to remove traces of acidity before use. CD_3CN was purchased from Euriso-TOP.

General Synthetic Procedures

Chemical synthesis was performed as detailed below and in the Supplemental Information (Synthesis and isolation section, see Figure S26 for chemical structures). See Figures S27–S42 for ^{1}H, $^{13}C\{^{1}H\}$, HMBC, ROESY, COSY, HSQC and CD spectra of all products.

Synthesis of $(LTV)_2A_3$

LTV (0.220 mg; 0.496 mmol) was dissolved in $CHCl_3$ (15 mL), then **A** (0.156 g; 0.744 mmol) in $CHCl_3$ (18 mL) was added dropwise over 5 min. The resulting clear, colourless solution was stirred for 72 h at room temperature. Then, 0.2 mg of Na_2SO_4 were added to the solution to remove as much water as possible. The suspension was filtered off and the resulting solution was dried at reduced pressure and low temperature (ca. 5-10 °C) to afford pure $(\mathbf{LTV})_2\mathbf{A}_3$ as a white solid.

Yield and Characterisation Data for $(LTV)_2A_3$

Yield: 0.259 g (74%); ^{1}H NMR (500 MHz, 25 °C, $CDCl_3$) δ 8.25 (s, 1H), 8.00 (s, 1H), 7.72 (d, *J* = 8.1 Hz, 2H), 6.48 (d, *J* = 7.8 Hz, 2H), 3.96 (t, *J* = 11.2 Hz, 1H), 3.62 (d, *J* = 7.9 Hz, 1H), 3.03 – 2.90 (m, 1H), 2.61 (d, *J* = 3.7 Hz, 2H), 2.22 (d, *J* = 7.1 Hz, 1H), 1.04 (d, *J* = 6.7 Hz, 3H), 0.81 (d, *J* = 6.6 Hz, 3H). $^{13}C\{^{1}H\}$ NMR (125 MHz, 25 °C, $CDCl_3$) δ 172.1, 162.9, 143.3, 134.6, 128.8, 127.9, 84.8, 57.2, 37.4, 33.0, 19.7, 19.6. HRMS (ESI+) m/z: $[M+2H]^{2+}$ calcd 705.4361, found 705.4387.

Synthesis of $(DTV)_2A_3$

DTV (0.226 g; 0.510 mmol) was dissolved in $CHCl_3$ (16 mL), then **A** (0.160 g; 0.765 mmol) in $CHCl_3$ (18 mL) was added dropwise over 5 min. The resulting clear, colourless solution was stirred for 72 h at room temperature. Then, 0.2 g of Na_2SO_4 were added to the solution to remove as much water as possible. The suspension was filtered off and the resulting solution was dried at reduced pressure and low temperature (ca. 5-10 °C) to afford pure $(\mathbf{DTV})_2\mathbf{A}_3$ as a white solid.

Yield and Characterisation Data for $(DTV)_2A_3$

Yield: 0.284 g (81%); ^{1}H NMR (500 MHz, 25 °C, $CDCl_3$) δ 8.25 (s, 1H), 8.00 (s, 1H), 7.72 (d, *J* = 8.1 Hz, 2H), 6.48 (d, *J* = 7.8 Hz, 2H), 3.96 (t, *J* = 11.2 Hz, 1H), 3.62 (d, *J* = 7.9 Hz, 1H), 3.03 – 2.90 (m, 1H), 2.61 (d, *J* = 3.7 Hz, 2H), 2.22 (d, *J* = 7.1 Hz, 1H), 1.04 (d, *J* = 6.7 Hz, 3H), 0.81 (d, *J* = 6.6 Hz, 3H). $^{13}C\{^{1}H\}$ NMR (125 MHz, 25 °C, $CDCl_3$) δ 172.1, 162.9, 143.3, 134.6, 128.8, 127.9, 84.8, 57.2, 37.4, 33.0, 19.7, 19.6. HRMS (ESI+) m/z: $[M+2H]^{2+}$ calcd 705.4361, found 705.4387.

Synthesis of $(LTF)_2A_3$

LTF (0.298 g; 0.507 mmol) was dissolved in $CHCl_3$ (16 mL), then **A** (0.159 g; 0.761 mmol) in $CHCl_3$ (18 mL) was added dropwise over 5 min. The resulting clear, colourless solution was stirred for 40 h at room temperature. Then, 0.2 g of Na_2SO_4 were added to the solution to remove as much water as possible. The suspension was filtered off and the resulting solution was dried at reduced pressure and low temperature (ca. 5-10 °C) to afford pure $(\mathbf{LTF})_2\mathbf{A}_3$ as a white solid.

Yield and Characterisation Data for $(LTF)_2A_3$

Yield: 0.379 g (88%); ^{1}H NMR (500 MHz, 25 °C, $CDCl_3$) δ 8.33 (dd, J = 7.9, 4.4 Hz, 1H), 7.64 – 7.50 (m, 3H), 7.09 – 6.99 (m, 3H), 6.88 (t, J = 7.5 Hz, 2H), 6.07 (d, J = 7.8 Hz, 2H), 4.21 (dd, J = 11.1, 2.6 Hz, 1H), 4.01 – 3.89 (m, 1H), 3.65 (dd, J = 13.4, 2.5 Hz, 1H), 3.05 – 2.94 (m, 1H), 2.94 – 2.79 (m, 2H), 2.64 – 2.54 (m, 1H). ^{13}C{^{1}H} NMR (125 MHz, 25 °C, $CDCl_3$) δ 172.9, 163.7, 143.3, 136.9, 134.1, 130.2, 128.8, 128.4, 128.0, 126.7 128.8, 127.9, 77.9, 56.8, 42.1, 39.1, 29.9. HRMS (ESI+) m/z: $[M+2H]^{2+}$ calcd 849.4372, found 849.4356.

Synthesis of $(DTF)_2A_3$

DTF (0.290 g; 0.493 mmol) was dissolved in $CHCl_3$ (15 mL), then **A** (0.155 g; 0.740 mmol) in $CHCl_3$ (18 mL) was added dropwise over 5 min. The resulting clear, colourless solution was stirred for 40 h at room temperature. Then, 0.2 g of Na_2SO_4 were added to the solution to remove as much water as possible. The suspension was filtered off and the resulting solution was dried at reduced pressure and low temperature (ca. 5-10 °C) to afford pure $(\mathbf{DTF})_2\mathbf{A}_3$ as a white solid.

Yield and Characterisation Data for $(DTF)_2A_3$

Yield: 0.377 g (90%); ^{1}H NMR (500 MHz, 25 °C, $CDCl_3$) δ 8.33 (dd, J = 7.9, 4.4 Hz, 1H), 7.64 – 7.50 (m, 3H), 7.09 – 6.99 (m, 3H), 6.88 (t, J = 7.5 Hz, 2H), 6.07 (d, J = 7.8 Hz, 2H), 4.21 (dd, J = 11.1, 2.6 Hz, 1H), 4.01 – 3.89 (m, 1H), 3.65 (dd, J = 13.4, 2.5 Hz, 1H), 3.05 – 2.94 (m, 1H), 2.94 – 2.79 (m, 2H), 2.64 – 2.54 (m, 1H). ^{13}C{^{1}H} NMR (125 MHz, 25 °C, $CDCl_3$) δ 172.9, 163.7, 143.3, 136.9, 134.1, 130.2, 128.8, 128.4, 128.0, 126.7 128.8, 127.9, 77.9, 56.8, 42.1, 39.1, 29.9. HRMS (ESI+) m/z: $[M+2H]^{2+}$ calcd 849.4372, found 849.4356.

X-Ray crystallography

LTV and $\mathbf{(LTF)_2A_3}$ X-Ray diffraction data was obtained on a 4-circle Xcalibur EosS2 diffractometer (Agilent Technologies) equipped with a CCD detector. CCDC numbers: 2143486 and 2143485, respectively. **DTV**, $\mathbf{(DTF)_2A_3}$ and $\mathbf{(DTV)_2A_3}$ X-Ray diffraction data was obtained on a SuperNova-Dual diffractometer (Agilent Technologies) equipped with an Atlas CCD detector. CCDC numbers: 2143483, 2143482, and 2143484, respectively. The structures were solved with the SHELXT 2014/5[77] structure solution program and refined with the SHELXL-2018/3[78] refinement package. Artwork representations were processed using MERCURY[79] software.

Single-crystals for the cryptands were obtained by slow diffusion (gas-liquid) of cyclohexane into a toluene:$CHCl_3$ solution of the desired macrobicycle.

See X-Ray crystallography details section in the Supplemental Information for additional information. Figures S43-S47 display thermal ellipsoid plots for all solid-state molecular structures.

DFT calculations

The X-ray geometric structures for the homochiral species were used as the starting point for Montecarlo conformational searches. The most stable conformation was initially determined at the MMFF level of theory using Spartano8 software,[80] and then the DFT models were calculated. The same procedure was followed for the heterochiral species, starting from the X-ray geometry of the homochiral species, and then modifying the three chiral centres of one of the cage lids.

DFT calculations were run with Gaussian 09 (revision B.01).[81] Geometry optimizations were carried out without symmetry restrictions at the B3LYP level,[82] using the Lanl2Dz basis set.[83] Analytical frequency calculations were used to characterise each stationary point as a minimum. These calculations, carried out at 298.15 K, also allowed for obtaining the thermal and entropic corrections required to calculate Gibbs energy differences.

See Computational details section in the Supplemental Information for additional information.

SUPPLEMENTAL INFORMATION

Supplemental Information (PDF) can be found online at https://doi.org/XXXXXXXX.

ACKNOWLEDGMENTS

This study is dedicated to the 80th birthday of Professor Alain Krief. We thank the ERC (Advanced Research Grant SUPRADAPT 290585) and the University of Strasbourg Institute for Advanced Study (USIAS) for financial support. This work was also supported by the projects UJI-B2019-40 (Pla de Promoció de la Investigació de la Universitat Jaume I) and RTI2018-098233-B-C22 (FEDER/Ministerio de Ciencia e Innovación – Agencia Estatal de Investigación). F.E. acknowledges MECD for a FPU fellowship (FPU 2017/02060) and for the mobility grant (EST19/00278). We thank Dr. Jean-Louis Schmitt and Dr. Cyril Antheaume for discussions of the NMR and mass spectral data as well as Dr. Artem Osypenko, Dr. Meixia He and Chengyi Zhu for extensive discussions.

.

AUTHOR CONTRIBUTIONS

Conceptualization: F.E., S.V.L., and J.-M.L.; resources: B.A., E.G.-V., S.V.L., and J.-M.L.; investigation: F.E.; DFT calculations: F.E.; writing—original draft: F.E.; writing—review and editing: F.E., S.V.L. and J.-M.L.; revision of the manuscript: F.E., B.A., E.G.-V., S.V.L., and J.-M.L.; funding acquisition: B.A., E.G.-V., S.V.L., and J.-M.L.; supervision: J.-M.L. and S.V.L.

DECLARATION OF INTERESTS

The authors declare no competing interests.

REFERENCES*

1. Yu, J., Qi, D., and Li, J. (2020). Design, synthesis and applications of responsive macrocycles. Commun Chem. *3*, 189. 10.1038/s42004-020-00438-2.
2. Pinalli, R., Pedrini, A., and Dalcanale, E. (2018). Biochemical sensing with macrocyclic receptors. Chem. Soc. Rev. *47*, 7006-7026. 10.1039/C8CS00271A.
3. Marsault, E., and Peterson, M. L. (2011). Macrocycles Are Great Cycles: Applications, Opportunities, and Challenges of Synthetic Macrocycles in Drug Discovery. J. Med. Chem. *7*, 1961-2004. 10.1021/jm1012374.
4. Dietrich, B., Viout, P., and Lehn, J.-M. (1993). Macrocyclic Chemistry: Aspects of Organic and Inorganic Supramolecular Chemistry (VCH).
5. Yang, J.-M., Yu, Y., and Rebek Jr, J. (2021). Selective Macrocycle Formation in Cavitands. J. Am. Chem. Soc. *143*, 2190-2193. 10.1021/jacs.0c12302.
6. Martí-Centelles, V., Pandey, M. D., Burguete, M. I., and Luis, S. V. Macrocyclization Reactions: The Importance of Conformational, Configurational, and Template-Induced Preorganization. Chem. Rev. *115*, 8736-8834. 10.1021/acs.chemrev.5b00056.
7. Vilar,R. (2008). Anion Templates in Synthesis and Dynamic Combinatorial Libraries (Springer), pp. 175-206.
8. Rossa, L., and Vögtle, F. (1983). Synthesis of Medio- And Macrocyclic Compounds By High Dilution Principle Techniques, F. Vögtle, eds. (Springer).
9. Lei, Y., Chen, Q., Liu, P., Wang, L., Wang, H., Li, B., Lu, X., Chen, Z., Pan, Y., Huang, F., and Li, H. (2021). Molecular Cages Self-Assembled by Imine Condensation in Water. Angew. Chem. Int. Ed. *60*, 4705-4711. 10.1002/anie.202013045.
10. Abet, V., Szczypinski, F. T., Little, M. A., Santolini, V., Jones, C. D., Evans, R., Wilson, C., Wu, X., Thorne, M. F., Bennison, M. J., et al. (2020). Inducing Social Self-Sorting in Organic Cages To Tune The Shape of The Internal Cavity. Angew. Chem. Int. Ed. *59*, 16755-16763. 10.1002/anie.202007571.
11. Komáromy, D., Nowak, P., and Otto, S. (2017). Dynamic Covalent Chemistry: Principles, Reactions and Applications (Wiley).
12. McKee, V., Nelson, J., and Town, R. M. (2003). Caged oxoanions. Chem. Soc. Rev. *32*, 309-325. 10.1039/B200672N.
13. McDowell, D., Nelson, J., and McKee, V. (1989). A furan-derived schiff-base crypt and incorporating the trans,trans dicarbimine link. Polyhedron *8*, 1143-1145. 10.1016/S0277-5387(00)81132-8.
14. Jazwinski, J., Lehn, J.-M., Lilienbaum, D., Ziessel, R., Guilhem, J., and Pascard, C. (1987). Polyaza Macrobicyclic Cryptands: Synthesis, Crystal Structures of a Cyclophane Type Macrobicyclic Cryptand and of its Dinuclear Copper(i) Cryptate, and Anion Binding Features. J. Chem. Soc. Chem. Commun. 1691-1694. 10.1039/C39870001691.
15. Yang, Z., and Lehn, J.-M. (2020). Dynamic Covalent Self-Sorting and Kinetic Switching Processes in Two Cyclic Orders: Macrocycles and Macrobicyclic Cages. J. Am. Chem. Soc. 142, 15137-15145. 10.1021/jacs.0c07131.
16. Greenaway, R. L., Santolini, V., Szczypiński, F. T., Bennison, M. J., Little, M., Marsh, A., Jelfs, K. E., and Cooper, A. I. (2020). Organic Cage Dumbbells. Chem. Eur. J. *26*, 3718-3722. 10.1002/chem.201905623.
17. Kołodziejski, M., Stefankiewicz, A. R., and Lehn, J.-M. (2019). Dynamic Polyimine Macrobicyclic Cryptands – Self-Sorting with Component

Selection. Chem. Sci. *10*, 1836–1843. 10.1039/C8SC04598D.

18. Vantomme, G., and Lehn, J.-M. (2014). Reversible Adaptation to Photoinduced Shape Switching by Oligomer-Macrocycle Interconversion with Component Selection in a Three-State Constitutional Dynamic System. Chem. Eur. J. *20*, 16188-16193. 10.1002/chem.201404561.

19. Acharyya, K., Mukherjee, S., and Mukherjee, P. S. (2013). Molecular Marriage through Partner Preferences in Covalent Cage Formation and Cage-to-Cage Transformation. J. Am. Chem. Soc. *135*, 554-557. 10.1021/ja310083p.

20. Ayme, J.-F., Lehn, J.-M., Bailly, C., and Karmazin, L. (2020). Simultaneous Generation of a [2 × 2] Grid-Like Complex and Linear Double Helicate: a Three-Level Self-Sorting Process. J. Am. Chem. Soc. *142*, 5819-5824. 10.1021/jacs.0c00896.

21. Roberts, D. A., Pilgrim, B. S., and Nitschke, J. R. (2018). Covalent Post-Assembly Modification in Metallosupramolecular Chemistry. Chem. Soc. Rev. *47*, 626-644. 10.1039/C6CS00907G

22. Wood, C. S., Ronson, T. K., Belenguer, A. M., Holstein, J. J., and Nitschke, J. R. (2015). Two-Stage Directed Self-Assembly of a Cyclic [3]catenane. Nat. Chem. *7*, 354–358. 10.1038/nchem.2205.

23. Beves, J. E., Campbell, C. J., Leigh, D. A., and Pritchard, R. G. (2013). Tetrameric Cyclic Double Helicates as a Scaffold for a Molecular Solomon Link. Angew. Chem. Int. Ed. *52*, 6464-6467. 10.1002/anie.201302634.

24. Uhlenheuer, D. A., Petkau, K., and Brunsveld, L. (2010). Combining supramolecular chemistry with biology. Chem. Soc. Rev. *39*, 2817-2826. 10.1039/B820283B.

25. Safont-Sempere, M. M., Fernández, G., and Würthner, F. (2011). Self-Sorting Phenomena in Complex Supramolecular Systems. Chem. Rev. *111*, 5784-5814. 10.1021/cr100357h.

26. Levy, Y., and Onuchic, J. N. (2004). Water and proteins: A love-hate relationship. Proc. Natl. Acad. Sci. U.S.A. *101*, 3325-3326. 10.1073/pnas.0400157101.

27. Zhao, X., Wang, H., Li, B., Zheng, B., Yang, D., Xu, W., Li, X., Yang, X.-J., and Wu, B. (2021). Narcissistic self-sorting in anion-coordination-driven assemblies. Chem. Commun. *57*, 6078-6081. 10.1039/D1CC01652K.

28. Coubrough, H. M., van der Lubbe, S. C. C., Hetherington, K., Minard, A., Pask, C., Howard, M. J., Fonseca Guerra, C., and Wilson, A. J. (2019). Supramolecular Self-Sorting Networks using Hydrogen-Bonding Motifs. Chem. Eur. J. *25*, 785–795. 10.1002/chem.201804791.

29. Aratsu, K., Prabhu, D. D., Iwawaki, H., Lin, X., Yamauchi, M., Karatsu, T., and Yagai, S. (2016). Self-sorting regioisomers through the hierarchical organization of hydrogen-bonded rosettes. Chem. Commun. *52*, 8211-8214. 10.1039/C6CC03419E.

30. Wu, A., and Isaacs, L. (2003). Self-Sorting: The Exception or the Rule?. J. Am. Chem. Soc. *125*, 4831-4835. 10.1021/ja028913b.

31. Chen, Y., Qian, C., Zhao, Q., Cheng, M., Dong, X., Zhao, Y., Jiang, J., and Wang, L. (2019). Adjustable chiral self-sorting and self-discriminating behaviour between diamond-like Tröger's base-linked cryptands. Chem. Commun. *55*, 8072-8075. 10.1039/C9CC03577J.

32. Liu, M., Zhang, L., and Wang, T. (2015). Supramolecular Chirality in Self-Assembled Systems. Chem. Rev. *115*, 7304–7397. 10.1021/cr500671p.

33. Jedrzejewska, H., and Szumna, A. (2017). Making a Right or Left Choice: Chiral Self-Sorting as a Tool for the Formation of Discrete Complex Structures. Chem. Rev. *117*, 4863–4899. 10.1021/acs.chemrev.6b00745.

34. Brandt, J., Salerno, F., and Fuchter, M. (2017). The added value of small-molecule chirality in technological applications. Nat. Rev. Chem. *1*, 0045. 10.1038/s41570-017-0045.

35. Luis, S. V., and Alfonso, I. (2014). Bioinspired Chemistry Based on Minimalistic Pseudopeptides. Acc. Chem. Res. *47*, 112–124. 10.1021/ar400085p.

36. Solà, J., Jimeno, C., and Alfonso, I. (2020). Exploiting complexity to implement function in chemical systems. Chem. Commun. *56*, 13273-13286. 10.1039/D0CC04170J.

37. Martí, I., Rubio, J., Bolte, M., Burguete, M. I., Vicent, C., Quesada, R., Alfonso, I., and Luis, S. V. (2012). Tuning Chloride Binding, Encapsulation, and Transport by Peripheral Substitution of Pseudopeptidic Tripodal Small Cages. Chem. Eur. J. *18*, 16728–16741. 10.1002/chem.201202182.

38. Gorla, L., Martí-Centelles, V., Altava, B., Burguete, M. I., and Luis, S. V. (2019). The role of the side chain in the conformational and self-assembly patterns of C2-symmetric Val and Phe pseudopeptidic derivatives. CrystEngComm *21*, 2398–2408. 10.1039/C8CE02088D.

39. Herschlag, D., and Pinney, M. M. (2018). Hydrogen Bonds: Simple after All?. Biochemistry *57*, 3338–3352. 10.1021/acs.biochem.8b00217.

40. White, N. G., Serpell, C. J., and Beer, P. D. (2014). Structural Study of Triazole and Amide Containing Anion-Templated Pseudorotaxanes. Cryst. Growth Des. *14*, 3472-3479. 10.1021/cg500420u.

41. Alvarez, S. (2013). A cartography of the van der Waals territories. Dalton Trans. *42*, 8617-8636. 10.1039/C3DT50599E.

42. Song, Z., Fu, H., Wang, R., Pacheco, L. A., Wang, X., Lin, Y., and Cheng, J. (2018). Secondary structures in synthetic polypeptides from N-carboxyanhydrides: design, modulation, association, and material applications. Chem. Soc.

Rev. *47*, 7401-7425. 10.1039/C8CS00095F.

43. Davis, J. M., Tsou, L. K.,and Hamilton, A. D. (2007). Synthetic non-peptide mimetics of α-helices. Chem. Soc. Rev. *36*, 326–334. 10.1039/b608043j.

44. Belowich, M. E., and Stoddart, J. F. (2012). Dynamic imine chemistry. Chem. Soc. Rev. *41*, 2003–2024. 10.1039/C2CS15305J.

45. Morris, K. F., and Johnson, C. S. (1992). Diffusion-ordered two-dimensional nuclear magnetic resonance spectroscopy. J. Am. Chem. Soc. *114*, 3139-3141. 10.1021/ja00034a071.

46. Bru, M., Alfonso, I., Burguete, M. I., and Luis, S. V. (2006). Anion-Templated Syntheses of Pseudopeptidic Macrocycles. Angew. Chem. Int. Ed. 45, 6155–6159. 10.1002/anie.200602206.

47. Curtis, N. F. (1968). Macrocyclic coordination compounds formed by condensation of metal-amine complexes with aliphatic carbonyl compounds. Coord. Chem. Rev. *3*, 3-47. 10.1016/S0010-8545(00)80104-6

48. Blackmond, D. G. (2020). Autocatalytic models for the origin of biological homochirality. Chem. Rev. *120*, 4831–4847. 10.1021/acs.chemrev.9b00557.

49. Bissette, A. J., and Fletcher, S. P. (2013). Mechanisms of autocatalysis. Angew. Chem. Int. Ed. *52*, 12800–12826. 10.1002/anie.201303822.

50. Jennings, W. B., Farrell, B. M., and Malone, J. F. (2001). Attractive Intramolecular Edge-to-Face Aromatic Interactions in Flexible Organic Molecules. Acc. Chem. Res. *34*, 885–894. 10.1021/ar0100475.

51. Song, B., Zhang, Z., Wang, K., Hsu, C.-H., Bolarinwa, O., Wang, J., Li, Y., Yin, G.-Q., Rivera, E., Yang, H.-B., et al. (2017). Direct Self-Assembly of a 2D and 3D Star of David. Angew. Chem. Int. Ed. *56*, 5258–5262. 10.1002/anie.201701417.

52. Leigh, D. A., Pritchard, R. G., and Stephens, A. J. (2014). A Star of David catenane. Nat. Chem. *6*, 978-982. 10.1038/nchem.2056.

53. Hasenknopf, B., Lehn, J.-M., Kneisel, B. O., Baum, G., and Fenske, D. (1996). Self-Assembly of a Circular Double Helicate. Angew.Chem. Int. Ed. Engl. *35*, 1838-1840. 10.1002/anie.199618381.

54. Chen, Y., Wu, G., Chen, B., Qu, H., Jiao, T., Li, Y., Ge, C., Zhang, C., Liang, L., Zeng, X., et al. (2021). Self-Assembly of a Purely Covalent Cage with Homochirality by Imine Formation in Water. Angew. Chem. Int. Ed. *60*,18815–18820. 10.1002/anie.202106428.

55. Gidron, O., Jirásek, M., Trapp, N., Ebert, M.-O., Zhang, X., and Diederich, F. (2015). Homochiral [2]Catenane and Bis[2]catenane from Alleno-Acetylenic Helicates - A Highly Selective Narcissistic Self-Sorting Process. J. Am. Chem. Soc. *137*, 12502-12505. 10.1021/jacs.5b08649.

56. Kramer, R., Lehn, J.-M., De Cian, A., and Fischer, J. (1993). Self-Assembly, Structure, and Spontaneous Resolution of a Trinuclear Triple Helix from an Oligobipyridine Ligand and Ni" Ions. Angew. Chem. Int. Ed. Engl. *32*, 703-706. 10.1002/anie.199307031.

57. Shoulders, M. D., and Raines, R. T. (2009). Collagen structure and stability. Annu. Rev. Biochem. *78*, 929–958. 10.1146/annurev.biochem.77.032207.120833.

58. Felsenfeld, G., Davies, D. R., and Rich, A. (1957). Formation of a three-stranded polynucleotide molecule. J. Am. Chem. Soc. *79*, 2023-2024. 10.1021/ja01565a074.

59. Felsenfeld, G., and Rich, A. (1957). Studies on the formation of two- and three-stranded polyribonucleotides. Biochim. Biophys. Acta *3*, 457-468. 10.1016/0006-3002(57)90091-4.

60. Ranjbar, B., and Gill, P. (2009). Circular Dichroism Techniques: Biomolecular and Nanostructural Analyses- A Review. Chem. Biol. Drug Des. *74*, 101–120. 10.1111/j.1747-0285.2009.00847.x.

61. Bulheller, B. M., Miles, A. J., Wallace, B. A., and Hirst, J. D. (2008). Charge-transfer transitions in the vacuum ultraviolet of protein circular dichroism spectra. J. Phys. Chem. B *112*, 1866–1874. 10.1021/jp077462k.

62. Kelly, S. M., Jess, T. J., and Price, N. C. (2005). How tostudy proteins by circular dichroism. Biochim. Biophys. Acta *1751*, 119–139. 10.1016/j.bbapap.2005.06.005.

63. Holub, J., Vantomme, G., and Lehn, J.-M. (2016). Training a Constitutional Dynamic Network for Effector Recognition: Storage, Recall, and Erasing of Information. J. Am. Chem. Soc. *138*, 11783–11791. 10.1021/jacs.6b05785.

64. Bru, M., Alfonso, I., Bolte, M., Burguete, M. I., and Luis, S. V. (2011). Structurally disfavoured pseudopeptidic macrocycles through anion templation. Chem. Commun. *47*, 283-285. 10.1039/C0CC01784A.

65. Beer, P. D., Sambrook, M. R., and Curiel, D. (2006). Anion-templated assembly of interpenetrated and interlocked structures. Chem. Commun. *20*, 2105–2117. 10.1039/B516435B.

66. Howlader, P., Mondal, S., Ahmed, S., Mukherjee, P. S. (2020). Guest-Induced Enantioselective Self-Assembly of a Pd6 Homochiral Octahedral Cage with a C3-Symmetric Pyridyl Donor. J. Am. Chem. Soc. *142*, 20968-20972. 10.1021/jacs.0c11011.

67. Wu, G., Chen, Y., Fang, S., Tong, L., Shen, L., Ge, C., Pan, Y., Shi, X., Li, H. (2021). Self-Assembled Cage for Wide-Scope Chiral Recognition in Water. Angew. Chem. Int. Ed. *60*, 16594–16599. 10.1002/anie.202104164.

68. Zarges, W., Hall, J., Lehn, J.-M., and Bolm, C. (1991). Helicity Induction in Helicate Self-Organisation from Chiral

Tris(bipyridine) Ligand Strands. Helv. Chim. Acta *74*, 1843-1852. 10.1002/HLCA.19910740827.

69. Yan, L.-L., Tan, C.-H., Zhang, G.-L., Zhou, L.-P., Bünzli, J.-C., and Sun, Q.-F. (2015). Stereocontrolled Self-Assembly and Self-Sorting of Luminescent Europium Tetrahedral Cages. J. Am. Chem. Soc. *137*, 8550-8555. 10.1021/jacs.5b03972.

70. Wang, J., Zhao, H., Chen, M., Jiang, Z., Wang, F., Wang, G., Li, K., Zhang, Z., Liu, D., Jiang, Z., and Wang, P. (2020). Construction of Macromolecular Pinwheels Using Predesigned Metalloligands. J. Am. Chem. Soc. *142*, 21691–21701. 10.1021/jacs.0c08020.

71. Beaudoin, D., Rominger, F., and Mastalerz M. (2017). Chiral Self-Sorting of [2+3] Salicylimine Cage Compounds. Angew. Chem. Int. Ed. 2017, 56,1244–1248. 10.1002/anie.201610782.

72. Shi, X., Fettinger, J. C., Cai, M., and Davis, J. T. (2000). Enantiomeric Self-Recognition: Cation-Templated Formation of Homochiral Isoguanosine Pentamers. Angew. Chem. Int. Ed. *39*, 3124–3127. 10.1002/1521-3773(20000901)39:17<3124::aid-anie3124>3.0.co;2-x.

73. Wang, X., Peng, P., Xuan, W., Wang, Y., Zhuang, Y., Tian, Z., and Cao, X. (2018). Org. Biomol. Chem. *16*, 34–37. 10.1039/C7OB02727C.

74. Beuerle, F., Klotzbach, S., and Dhara, A. (2016). Let's Sort It Out: Self-Sorting of Covalent Organic Cage Compounds. Synlett 27,1133–1138. 10.1055/s-0035-1561364.

75. Ernst, J. A., Clubb, R. L., Zhou, H.-X., Gronenborn, A. M., and Clore, G. M. (1995). Demonstration of Positionally Disordered Water Within a Protein Hydrophobic Cavity by NMR. Science *267*, 1813-1817. 10.1126/science.7892604.

76. Kyte, J., and Doolittle R. F. (1982). A Simple Method for Displaying the Hydropathic Character of a Protein. J. Mol. Biol. 157, 105-132. 10.1016/0022-2836(82)90515-0.

77. Sheldrick, G. M. (2008). A short history of SHELX. Acta Crystallogr., Sect. A: Found. Crystallogr. *64*, 112-122. 10.1107/S0108767307043930.

78. Sheldrick, G. M. (2015). Crystal structure refinement with SHELXL. Acta Crystallogr., Sect. C: Struct. Chem. *71*,3-8. 10.1107/S2053229614024218.

79. Macrae, C. F., Bruno, I. J., Chisholm, J. A., Edgington, P. R., McCabe, P., Pidcock, E., Rodriguez-Monge, L., Taylor, R., van de Streek, J., and Wood, P. A. (2008). Mercury CSD 2.0 – new features for the visualization and investigation of crystal structures. J. Appl. Crystallogr. *41*, 466-470. 10.1107/S0021889807067908

80. Note: see https://www.wavefun.com/ for details

81. Frisch, M. J., Trucks, G. W., Schlegel, H. B., Scuseria, G. E., Robb, M. A., Cheeseman, J. R., Scalmani, G., Barone, V., Mennucci, B., Petersson, G. A., et al. (2010). Gaussian 09, Revision B.01 (Gaussian, Inc).

82. Becke, A. D. (1993). Density - functional thermochemistry. III. The role of exact exchange. J. Chem. Phys. *98*, 5648-5652. 10.1063/1.464913.

83. Chiodo, S., and Sicilia, E. (2006). LANL2DZ basis sets recontracted in the framework of density functional theory. J. Chem. Phys. *125*, 104107. 10.1063/1.2345197.

.